Nanoscale

Structural and Spectroscopic Characterization of Pyrene Derived Carbon Nano Dots: A Single-Particle Level Analysis

Journal:	*Nanoscale*
Manuscript ID	NR-ART-10-2021-007190.R2
Article Type:	Paper
Date Submitted by the Author:	13-Feb-2022
Complete List of Authors:	Batra, Gayatri; Deutsches Elektronen-Synchrotron Sharma, Shubham; Indian Institute of Technology Mandi Advanced Materials Research Center, School of Basic Sciences Kaushik, Kush; Indian Institute of Technology Mandi Advanced Materials Research Center, School of Basic Sciences 175005 Rao, Chethana; Indian Institute of Technology Mandi, School of Basic Sciences Kumar, Pawan; University of Pennsylvania, Materials Science and Engineering Laboratory for Research on the Structure of Matter University of Pennsvylania, USA 19104 Kumar, Krishan; Indian Institute of Technology Mandi Advanced Materials Research Center, School of Basic Sciences 175005 Ghosh, Subrata; Indian Institute of Technology Mandi, School of Bsic Sciences Jariwala, Deep; University of Pennsylvania, Electrical and Systems Engineering Stach, Eric; University of Pennsylvania, Materials Science and Engineering Yadav, Aditya; IIT Mandi, SBS Nandi, Chayan; IIT Mandi, SBS

Structural and Spectroscopic Characterization of Pyrene Derived Carbon Nano Dots: A Single-Particle Level Analysis

Gayatri Batra,[1, 2, ¥]¶ *Shubham Sharma,* [1, 2]¶ *Kush Kaushik,* [1, 2] *Chethana Rao,* [1, 2] *Pawan Kumar,* [3,4] *Krishan Kumar,* [1, 2] *Subrata Ghosh,* [1, 2] *Deep Jariwala,* [3] *Eric A. Stach,*[4] *Aditya Yadav*[1, 2] * *and Chayan Kanti Nandi*[1, 2] *

[1]School of Basic Sciences, Indian Institute of Technology, Mandi, HP-175001, India.

[2]Advanced Materials Research Centre, Indian Institute of Technology, Mandi, HP-175001, India.

[3]Department of Electrical and Systems Engineering, University of Pennsylvania, Philadelphia, PA-19104

[4]Department of Materials Science and Engineering, University of Pennsylvania, Philadelphia, PA-19104

Current address

[¥]Deutsches Elektronrn-Synchrotron (DESY), Notkestraße 85, 22607, Hamburg, Germany

¶*Gayatri Batra and Shubham Sharma have contributed equally to the work*

Abstract

The bottom-up approach has been widely used for large-scale synthesis of carbon nanodots (CNDs). However, the structure and origin of photoluminescence in CNDs synthesized by the bottom-up approach is still a subject of debate. Here, using a series of separation techniques like solvent extraction, column chromatography, gel electrophoresis and dialysis, we present three distinct fluorescent components in CNDs synthesized from pyrene, a well-known precursor molecule. The separated components have qualitative and quantitatively different absorption and emission spectral features including quantum yield (QY). Optical and vibrational spectroscopy techniques combined with electron microscopy indicate that a subtle balance between the extent of graphitization and the presence of molecular fluorophores determines the nature of fluorescence emission. A substantial difference in photons/cycle, single-particle fluorescence blinking, on-off photoswitching strongly supports the distinct nature of the components.

Keywords: Carbon nanodots, bottom-up synthesis, pyrene derivative, molecular fluorophore, single-particle spectroscopy.

Introduction

Carbogenic nanodots, a new class of particulate nanomaterial is being widely explored in the field of bioimaging, optoelectronics, photovoltaics etc. owing to their superior optical properties such as high emission quantum yield in addition to aqueous solubility and low toxicity.[1–6] These nanodots could be classified into two categories based on their structure, namely carbon nanodots (CNDs) and graphene quantum dots (GQDs).[7,8] Structurally, both have a similar size of 2-5 nm with sp^2 hybridized graphitic carbon core, embedded by sp^3 hybridized epoxy, hydroxy, oxide and carboxyl functional groups. While CNDs can have 8-10 crystalline or amorphous graphene layers in their core structure, GQDs, by definition, consist of an atomically thin single graphene layer with armchair and/or zigzag edges.[9–12] Top-down and bottom-up approaches are the two main approaches for the synthesis of these dots. In the top-down method, bulk graphitic materials are used as precursors and are cut into small-sized CNDs or GQDs.[6,13–15] Unfortunately, this method often produces material with inhomogeneous size distributions. One of the most intriguing properties of these dots is their excitation dependent multicolor photoluminescence.[16–20] Several mechanisms have been proposed to explain these unusual emission characteristics. While the quantum confinement induced bandgap opening and edge state induced emission have been proposed as plausible explanations, the widely varying emission mechanisms of these dots is still a subject of investigation.

Recently, bottom-up approaches have been extensively studied to synthesize high quantum yield (QY) of both dots.[21,22] These are synthesized from small organic molecules via solvothermal and microwave synthesis. In these approaches, the reaction conditions such as temperature, reaction time, and precursor molecule play a significant role in determining the actual amount of GQDs or CNDs in the synthesis products.[23,24] For example, upon increasing the temperature or reaction time, the amount of graphitization was found to be increased and a clear shift from excitation independent to excitation dependent photoluminescence with a decrease in QY was observed. Even though the origin of excitation wavelength dependent, multicolor photoluminescence is still unclear, numerous recent reports have shown excitation independent photoluminescence in these dots.[25–27] Several hypotheses, including the presence of molecular fluorophores and/or their aggregated structure, quasi-CNDs/GQDs (molecular fluorophores attached to the graphitic core), which are produced as by-products or even as the sole product have been proposed to be present in the synthesis products and contribute to the luminescence.[9,28,29] For example, the formation of HPPT, a molecular fluorophore with green emission in CNDs solution was reported when synthesized from citric acid and urea as precursor molecules in microwave assisted pyrolysis.[31] Recently, separation of three components in CNDs solution derived from citric acid and urea was reported.[30] Interestingly, along with the green emissive HPPT, oligomeric urea with blue emission was found to be one of the separated components. A fine black powder that did not exhibit any significant emission also found as the third component.[31] Nevertheless, the formation of molecular fluorophore is majorly reported when citric acid is used as a precursor molecule. However, considering the vast synthesis protocols, elucidating the relationship between structure and luminescence properties in these dots synthesized using other highly utilized precursor molecules is of utmost importance.

Pyrene is one of the most well-known precursor molecules which has been extensively utilized for the synthesis of such dots. Synthesis of both CNDs and GQDs using pyrene as a precursor molecule is well reported in the literature.[32–44] Nevertheless, the optical origin of these dots still remains unclear and a detailed investigation will be critical for their future prospect. Herein, by using a series of separation techniques such as solvent extraction, gel-electrophoresis, thin-layer and column chromatography, we showed that, CNDs derived from pyrene contained three distinct emission components with their different weight percentages in the synthesis mixture. These components showed bright green, greenish brown and deep brown color when illuminated by 365 nm UV light. They have different absorption and emission spectral features and have completely different QY. The bright green color material is associated with the monomer and isomers of hydroxyl (OH)/carboxylic acid (COOH)/nitro (NO_2) functionalized pyrene derivative and has the highest QY. The greenish brown material is associated with quasi-CNDs like structure and has a moderate QY, while the deep brown colored material is pure CNDs like structure and has the lowest QY. Single-particle level analysis shows that emission characteristics such as photon counts/cycle, ON-OFF switching cycle, and single-particle blinking were all different in these components and strongly supporting the distinct nature of the materials.

Results and discussion

Synthesis and characterization of the pyrene derived CNDs:

CNDs were synthesized via the hydrothermal method by following a reported protocol for the gram-scale synthesis using pyrene as the precursor molecule.[45] The detailed synthesis procedure of CNDs is discussed in the **supporting information**. Briefly, pyrene was converted to 1,3,6-trinitropyrene (TNP) using nitration of 1 g pyrene in 80 ml nitric acid (HNO_3) at 80 °C for overnight (**Figure 1a**). The optical and chemical characterization of both pyrene and TNP are presented in **Figure S1-S6**. In the next step, 0.15 g of TNP was added to 60 ml 0.2 M NaOH solution and probe sonicated for 2 h to disperse the TNP in the solution. The mixture was then transferred to a hydrothermal reactor and heated at 200 °C for 10 h. After cooling down the mixture to room temperature, it was then filtered through a 0.22 μm polyvinylidene difluoride microporous membrane to remove large debris and unreacted material, if any. The obtained solution was freeze-dried to get solid brown CNDs.

The as-synthesized CNDs (crude) appeared light brown when examined through the naked eye upon dissolving into water but changed to green color under 365 nm UV-light illumination (**Figure 1a; top right**). Typically, in CNDs, those are synthesized via top-down method from solid graphitic precursor material (**details in supporting information**), the absorption spectra show exponential decay with maximum absorption below 400 nm. The spectrum generally consists of a π-π* core-state transition below 300 nm and n-π* surface/edge states transitions (C-O, C=O) in the range of 300-400 nm. Along with the above-discussed absorption features, the absorption spectra of the pyrene derived CNDs show intense vibronic progression peaks above 400 nm (**Figure 1b**). These peaks are very similar to molecular state absorption. The appearance of these new peaks suggests that apart from the core and edge state absorptions, the pyrene-derived CNDs have an additional molecular state like absorption.[46–48]

The emission spectra (**Figure 1c**) showed an excitation wavelength independent emission, with a maximum peak at 515 nm and a shoulder peak at 450 nm. This is quite unusual as CNDs are reported to show excitation wavelength dependent emission spectra, although this is a topic of debate. It is interesting to mention here that while the intensity of the 450 nm peak is observed to be higher than the 515 nm peak when excited within 300-380 nm, a switchover of intensity profile from 450 nm to 515 nm occurs when excited above 400 nm. The observed excitation wavelength independent emission features at 515 nm have a close resemblance with emission spectra for organic molecular fluorophore, which follow the fundamental rules of excited state emission.[49] As a result, in correlation with the absorption spectra and its transitions, the emission spectral features appearing at 450 nm in our case likely arise from the core and edge state emission, while the 515 nm emission features are likely molecular state-like emission. The measured fluorescence lifetime of the synthesized mixture was found to be 3.12 ns (**Figure S7**).

To further understand and isolate the source of emission, we carried out structural characterizations to gain a deeper insight into the atomic structure, chemical bonding Rand composition of the material. Powder x-ray diffraction (PXRD) of the sample shows a broad peak at ~26 degrees, a typical signature for CNDs (**Figure 1d**). Transmission electron microscopy (TEM) data shows a homogeneous particle size distribution of CNDs with a diameter of ~4 nm (**Figure 1e**). On the contrary, in Raman spectroscopy, instead of the characteristic D (defect) and G (graphitic) vibrational bands for CNDs, an intense fluorescence background was observed (**Figure 1f**). Surprisingly, the baseline correction of the spectrum resulted in the desired D and G bands,[50] although with lower intensity than expected. It is worth pointing out here that the intensity of the D band is almost half of the G band, suggesting a higher degree of crystallinity in the material. Nevertheless, the observed strong fluorescence background suggests that the synthesized CNDs have a substantial amount of highly emissive impurities such as molecular fluorophores, along with the presence of graphitic material in the synthesis mixture. We carried out both Fourier transform infrared (FTIR) and X-ray photoelectron spectroscopy (XPS) measurements to extract detailed information on the surface and buried functional groups in the synthesized CNDs products. **Figure 1g** shows the comparison of the FTIR spectra of the synthesized CNDs with TNP for a better understanding of the evolution of the functional groups. A broad peak at ~3430 cm^{-1} in the FTIR spectrum and ~1262 cm^{-1} peak corresponds to OH vibrational band (**Figure 1g**). The peaks at 1587 cm^{-1} and 1450 cm^{-1} could be attributed to the C=C bond. The broad peak at ~1650 cm^{-1} supports the presence of COOH group functional groups in the material. The survey XPS spectrum shows strong signals of C1s at 285.29 eV, and O1s peaks at 532.05 eV and a weak signal of N1s at 400 eV (**Figure S8**). The high-resolution spectrum of C1s and O1s confirms the C=C, C=O, C-OH and COOH functional groups, as observed in the FTIR spectra.[51–54]. The weak peak of N1s suggests that a small amount of nitrogen related functional group ($-NO_2$) still may be present.

Purification and characterization of as-synthesized CNDs:

The observations of molecular state like transitions in both the absorption and emission spectra, excitation wavelength independent emission spectra and strong fluorescence background in Raman spectrum encouraged us to carry out a systematic purification of the synthesized CNDs and characterize each of the separated components to pinpoint the structure-emission property relations. We performed various purification techniques such as solvent extraction, gel-electrophoresis as well as thin-layer and column chromatography. In the solvent extraction method, the crude product was dispersed in MeOH. The dissolved products were taken away every 24 hours by adding a fresh solvent set for eight days. It was found that a small amount (~3%) of the products remain entirely undissolved (**Figure 2a**).

We then carried out thin-layer chromatography (TLC) of the MeOH dissolved material using a 4:1 ratio of DCM/MeOH as mobile phase. Two separate spots were clearly visible when TLC paper was illuminated under 365 nm UV light (**Figure 2a; right**). Surprisingly, the TLC of the MeOH insoluble product left with only one immovable component. Next, we carried out column chromatography of the MeOH soluble products using silica as a stationary and DCM/MeOH as a mobile phase. Here, two separate components were eluted out from the column at 10:1 (32% weight of total crude products) and 5:1 (65% weight of total crude products) ratios of DCM/MeOH, respectively (**Figure 2b**). Unfortunately, we could not perform column chromatography of the MeOH insoluble material as it clogged the column. Nevertheless, it can be concluded that the as-synthesized CNDs product contains three different components with their different polarities and these are most probably present as different optical and chemical entities. Inset of **Figure 2c and 2d** represent the normal and 365 nm UV light illuminated color of the components. The observed 365 nm UV illuminated colors of the components are depicted as bright green, greenish brown and deep brown.

Optical characterization of the purified components:

We carried out detailed optical and chemical characterization for each of these components. The optical measurements were done both in well-dispersed bulk solutions and at single-particle level (detail of experimental procedures are in the **supporting information** and the results are discussed later). The absorption spectra of all three components are presented in **Figure 2c.** Remarkably distinct absorption spectral features for all of the three components were observed. The absorption spectra, similar to **Figure 1b**, categorically could be assigned to three different regions. The greenish brown component has intense absorption bands both below 300 nm (~262 nm) and above 400 nm, respectively. The absorption in the range of 300-400 nm is not prominent for this component. The magnified version (**Figure S9**) of the absorption spectra shows that the bright green component resembles the absorption spectra closely with the greenish brown component with a little variation in the vibronic band intensity above 400 nm. On the other hand, the deep brown component has strong absorption below 400 nm, as typically observed in CNDs, with a hinged peak at 236 nm and 355 nm. In addition, it has a much less structured absorption after 400 nm, although with a small hinged peak at around 485 nm. All the above observations suggested that these components are fundamentally different by their ground state structure. Therefore, by looking at the absorption spectra, one could directly differentiate between the various components synthesized during the CNDs synthesis.

Next, the emission spectra of all three components were recorded. The normalized emission spectra (**Figure 2d**) show a prominent and gradual redshift of the emission maxima from bright green to greenish brown to deep brown color components of the CNDs products when excited at a fixed wavelength of 460 nm. While the emission maxima obtained at 515 nm for the bright green component, the emission maxima obtained for greenish brown and deep brown components are at 525 nm and 541 nm respectively. We calculated the absolute QY by the integrated sphere method (**supporting information**). A substantial decrease in the QY from bright green (QY= 12%) to greenish brown (QY= 8%) to deep brown component (QY = 0.8%) was observed. The bright green and greenish brown components showed an average lifetime of 4.3 and 3.8 ns, while the average lifetime for the deep brown component was 0.41 ns (**Figure 2e**). The decrement in the lifetime from bright green (4.3 ns) to the greenish brown and deep brown components (3.8 ns and 0.41 ns) and the decrement in the QY suggest a decreasing radiative decay rate and increasing non-radiative decay rate. The extensive formation of C=C network in deep brown component could be attributed for generating non-radiative trap states leading to a decrease in lifetime value.[55]

Raman, TGA, FTIR and HRMS analysis of the purified components:

The emission spectral shifting in **Figure 2d**, at first glance, could be proposed as originating from a size-dependent quantum confinement effect, as reported earlier in CNDs. However, the measured Raman spectra and the thermogravimetric analysis (TGA) showed interesting and contradictory results. One of the most intriguing observations in the Raman spectra (**Figure 2f**) is that both the greenish brown and deep brown components show prominent D and G bands, while the bright green component shows only a fluorescence background. Unlike the crude sample, the bright green component shows no signatures of the D and G bands, even after baseline correction. On the other hand, the bright green component shows (**Figure 2g**) a gradual but significant mass loss (more than 60%) within 500 °C and then a prolonged mass loss till 1000 °C in TGA measurement. It should be pointed out here that the precursor molecule pyrene showed a complete mass loss at 200 °C and TNP showed extensive mass loss at around 350 °C (**Figure S10**). Based on these results, the bright green component is attributed to a pyrene derived molecular fluorophore. Conversely, the deep brown component displays a very high thermal stability. The greenish brown component showed lesser stability than deep brown but more stable than the bright green component. We also have recorded the FTIR spectra of all the separated components, to gain further insight into structural interpretation (**Figure 2h**). An intense band at 1415 cm^{-1} for deep brown component suggests the presence of an extensive network of C=C, which is almost absent in greenish brown and bright green components. A slight shift in the peak position from 1450 cm^{-1} to 1415 cm^{-1} for C=C bond vibration from crude CNDs to deep brown component could be attributed to the extended conjugation formed in the core structure. The decrease in binding energy of the C=C bond from 286.39 eV to 285.879 eV and the increase in atomic percentage from 9.46 to 17.67 (**Table S1**) supports the above change in the FTIR spectra. Furthermore, a moderate vibration peak at 1643 cm^{-1} and a broad vibration peak at 3408 cm^{-1} were observed for bright green and greenish brown components. These correspond to C=O and O-H stretching respectively. Surprisingly, both these peaks were found to be significantly less intense in deep brown component. Combining the analysis of Raman, TGA and FTIR results, it could be concluded that the deep brown component is comprised essentially of a large amount of carbon core but with less molecular fluorophore attached in it, while more functional groups but very less or no carbon core is present in the greenish brown and bright green components.

The mass spectra (positive mode) analysis of the separated components tentatively predicted the possible structure of the molecular fluorophores in bright green components, which are attached to the surface of the greenish brown and deep brown components (**Figure S11**). Deep brown component showed the mass peak at m/z = 308 $(C_{17}H_9NO_5 + H)^+$, m/z = 330 $(C_{17}H_9NO_5 + Na)^+$, m/z = 341 $(C_{19}H_{10}O_6 + Li)^+$ and m/z = 359 $(C_{17}H_8N_2O_6 + Na)^+$ (**Figure S12**) respectively. The mass spectra of greenish brown component showed a peak at m/z = 302 $(C_{16}H_9NO_4 + Na)^+$, m/z = 330 $(C_{17}H_9NO_5 + Na)^+$ and m/z = 360 $(C_{16}H_7N_3O_6 + Na)^+$ (**Figure S13**) respectively. The mass spectra of bright green component showed peak at m/z = 302 $(C_{16}H_9NO_4 + Na)^+$, m/z = 308 $(C_{17}H_9NO_5 + H)^+$ and m/z = 358 $(C_{18}H_9NO_6 + Na)^+$ (**Figure S14**). Hence, the mass spectral data suggested the possibility of the presence of a large pool of pyrene derivatives (**Figure S11**) with functional groups -OH/COOH/NO_2 or their structural isomers as molecular fluorophores. This is possibly due to the synthesis condition as reported earlier.[9]

Structural analysis by TEM, STEM and SEM:

For an in-depth structural characterization, we carried out transmission electron microscopy (TEM) and aberration-corrected (probe) scanning TEM (STEM) of all three components for direct visualization of the structure of our products at atomic resolution. TEM images of the bright green component do not show any particle features specific or analogous to CNDs. Instead, it depicts a variety of aggregated structures. Images of distinct morphologies were observed for the bright green component under different environmental conditions. For example, TEM indicates that the component has either a stacked, thread or ribbon-like structure (**Fig. 3a, b**). Such structures are likely aggregations of the molecular fluorophore. Various aggregated morphologies made up of the bright green component are further confirmed by scanning electron microscope (SEM) images (**Figure S15**). In addition, the material gets either burned or appeared blurry in contrast after few continuous scans during STEM imaging, supporting our hypothesis that it comprises an organic fluorophore structure that is less stable under the electron beam (**Figure 4a**). The greenish brown component showed fewer dot-like structures in some places of the grid under TEM (**Figure 3c, d**). The STEM images showed the highly bright white shadow throughout the grid with few dots like structures (**Figure 4b & d)**. These observations suggest the formation of CNDs with an abundant presence of fluorophore attached to it. In fact, on free-hanging places in the lacey grid, the greenish brown component is attached to these organic fluorophores, which do not allow imaging at atomic-scale resolution (**Figure S16**). On the contrary, the deep brown component showed many dot-like structures with an average size of 3.5 nm under TEM (**Figure 3e, f**). The high-resolution images showed distinct fringe contrast with a d-spacing of 0.21 nm for 001 plane of graphitic carbon in the image suggesting the presence of some crystalline order.[9] The STEM images showed the explicit crystalline nature of the CNDs with the size of 3.5 nm and d-spacing of 0.21 nm for 001 plane of graphitic carbon (**Figure 4c & e**). Electron energy loss spectra (EELS) from **Figure 4d** (**Figure 4f top**) shows a strong signature of oxygen in the greenish brown component thereby suggesting a hybrid structure of carbogenic core covered with oxygen containing organic functional groups on the surface. In contrast, the EELS from **Figure 4e** (**Figure 4f bottom**) showed a drastic reduction of oxygen functionality in the deep brown colored component.

Excitation wavelength dependent emission and structural analysis:

A defining feature of CNDs is their excitation wavelength dependent emission spectra. We measured the excitation wavelength dependent fluorescence from each of the three separated components (**Figure 5**). Surprisingly, instead of the commonly observed excitation dependent emission, all three components showed excitation wavelength independent emission with a peak maximum above 500 nm. The bright green component showed intense emission above 500 nm with a negligible emission below this wavelength upon excitation from 280 to 500 nm (**Figure 5a**). The greenish brown component also showed intense emission above 500 nm. However, a moderately intense but structured emission was also observed below 500 nm

(**Figure 5b**). On the other hand, the deep brown component showed almost equally intense emission both above and below 500 nm (**Figure 5c**). It is worth mentioning that, irrespective of the excitation wavelength, the bright green component always showed the emission peak at 515 nm, increasing its intensity from 320 to 480 nm excitation. On the contrary, the greenish brown and deep brown components showed prominent emission intensity below 500 nm when excited within 320 to 400 nm and a switchover of the intensity happened (from below 500 nm to above 500 nm emission) at around 400 nm or above excitation. From the above-mentioned spectral features, it could be concluded that, in all the components, the excitation independent emission mainly arises due to molecular fluorophore state emission, while the edge and core state is increased in greenish brown component and maximum in deep brown component. Possibly because of the presence of a large number of pyrene derivatives along with many different structural isomers as shown in **Figure S11** we were not able to get either single-crystal data or interpretable NMR data of the suggested fluorophores. Hence, our prediction on possible chemical structures of the fluorophores are based on the measured XPS (**Figure S17-S19**) and mass spectral data (**Figure S12-S14**), and the analysis revealed the presence of a considerable number of OH, COOH and a small number of NO_2 functional groups in the components. In addition, the time-resolved fluorescence anisotropy measurement provided the hydrodynamic diameter of the bright green component as 0.8 nm, which is actually the size of a molecular fluorophore (**Figure S20**). From all the above data, it could be concluded that the bright green component is OH/COOH/NO_2 functionalized pyrene derivative molecular fluorophore. The greenish brown component is assigned as a quasi-CNDs like structure, where the molecular fluorophores are attached to the edges of the core of CNDs (**Figure 5e**). A similar theoretical interpretation of the monomeric and dimeric forms of perylene on the surface of CNDs has been reported recently.[56] It is to be pointed out here that, this component has the maximum weight percentage (65%) with a high QY of 8% and a high lifetime of 3.8 ns. On the other hand, the deep brown component is the real crystalline CNDs with very low QY, and lesser fluorophores are attached to it (**Figure 5f**). In addition, it has little excitation dependency in the core and edge states emission (**Figure 5c**). Based on the above observations, it could be concluded that a large amount of highly intense bright green molecular fluorophore (weight percentage of 32%) with QY of 12% mainly dictates the green color emission in pyrene derived CNDs as presented in **Figure 1**.

We also carried out the gel electrophoresis separation and dialytic separation of the synthesized CNDs to check the feasibility of our results. Interestingly, we got the same three emissive components in the agarose gel. The optical absorption and emission spectra closely resemble the column purified bright green, greenish brown, and deep brown color components (**Figure S21**). The bright green component doesn't show any D and G bands in the Raman spectrum, while they were observed in the greenish brown and deep brown components with intensity increase in the deep brown component. The dialytic separation of the crude CNDs was carried out using 1 kDa membrane (**Figure S22**). While the dialysate showed all the features of the bright green component, the retentate showed the characteristic of greenish brown and deep brown CNDs. It is obvious as 1 kDa membrane will allow coming out only the smaller size molecular fluorophore, keeping the larger size CNDs inside. The measured Raman spectra showed the prominent D & G bands for retentate but not in the dialysate. The broad peak in PXRD also confirmed the CNDs like structure in the retentate. On the other hand, excitation independent emission was observed for dialysate, while both excitation independent and dependent emission was observed for the retentate.

Single-particle study of the purified components and cell imaging:

The single-particle level study of all three separated components were carried out in a homebuilt setup, equipped with 100x, oil immersion, 1.49NA, TIRF objective (Nikon) and 488 nm laser (Toptica). Details have been discussed in the **supporting information**. The data were analyzed by Andor Solis software with the help of home-written MATLAB code and Origin 2018 Pro. The measured real-time traces, photon/cycle, ON-OFF switching cycles and single-particle blinking were analyzed and presented in **Figure 6**. We analyzed approximately hundred real-time trace data for each of these components. Interestingly, photon/cycle values were obtained as 2484 for the bright green component, 746 for the greenish brown component and 536 for the deep brown component (**Figure 6a-c**). On the other hand, the ON-OFF switching cycles were found to be maximum in greenish brown component (43 cycles), while it was least (18 cycles) for the bright green component and 30 cycles for the deep brown component (**Figure 6d-f**). The photon/cycle data obtained at the single-particle level is in accordance with the bulk absolute QY, wherein the bright green component has the maximum QY, but the deep brown component has the least QY. Considering the very high switching cycles along with moderate photons/cycle, the greenish brown component has a QY of 8%. We also calculated the single-step bleaching and single-particle blinking events of these components (**Figure 6g-i**). Interestingly, blinking events, as high as ~80%, were observed for the greenish brown and deep brown components. On the other hand, the bright green component showed a lesser extent of blinking events (60%). The high blinking events, high ON-OFF switching suggested that each of these components have the potential application in localization-based super-resolution microscopy. Finally, we checked the bioimaging of these components. The HeLa cells were incubated for 12 hours by each of the three samples. Confocal microscopy images show that all the materials have the high capability to stain and image the cells with high brightness (**Figure S23**). While the bright green component showed the confocal image only in the green channel, the deep brown CNDs have the capability to get the image in red channel as well.

Conclusion

We unveiled three distinct bright green, greenish brown and deep brown-colored materials in the pyrene derived bottom-up approach hydrothermally large-scale synthesized CNDs. A series of separation techniques were applied to obtain the highly pure materials. We showed that the subtle balance between the extent of graphitization and the amount of the synthesized molecular fluorophores decides the nature of the fluorescence emission. Each separated component has a different emission, QY and a different weight percentage in the synthesis mixture. The bright green color material is supposed to originate from various isomers of OH/COOH/NO_2 functionalized pyrene derivatives with the highest QY among all the components and is mainly responsible for the emission color of the crude CNDs products. The greenish brown material is quasi-CNDs like structure with moderate QY and the deep brown color material is pure CNDs like structure with the lowest QY. Single-particle level fluorescence analysis shows that emission characteristics such as photon counts/cycle, ON-OFF switching cycle, and single-particle blinking were all different in these components and thus strongly supporting the distinct nature of the components. Our results unveil the true structural characterization and the source of emission of differently purified components of CNDs derived from a well-known precursor molecule Pyrene.

Supplementary Materials

The Supporting Information contains details of the experimental procedures, methods and characterizations.

Acknowledgments

CKN is thankful to (SERB) core research grant (CRG) India for the project number CRG/2020/000268 and the facilities of the AMRC and BioX center of IIT Mandi, India. Aditya Yadav thanks the Council of Scientific and Industrial Research, India [CSIR SRF:09/1058(0014)/2019-EMR-I]. Shubham Sharma thanks the University Grants

Commission, India [(16-9(June 2019)/2019(NET/CSIR)]. The STEM work was carried out at the Singh Center for Nanotechnology at the University of Pennsylvania which is supported by the National Science Foundation (NSF) National Nanotechnology Coordinated Infrastructure Program grant NNCI-1542153 as well as University of Pennsylvania Materials Research Science and Engineering Center (MRSEC). D.J., E.A.S., and P.K. acknowledge primary support for this work from U. Penn MRSEC seed grant supported by the NSF (DMR-1720530) and NSF DMR Electronic Photonic and Magnetic Materials (EPM) core program grant (DMR-1905853).

Author contributions

Gayatri Batra and Shubham Sharma performed all the synthesis, purification, characterization of the materials. Kush Kaushik conducted the single-particle level and absolute quantum yield measurement. Chethana Rao performed the TEM and SEM measurements. Pawan Kumar performed the STEM and EELS measurements. Krishan Kumar performed the ^{1}H NMR and HRMS study under the guidance of Subrata Ghosh. Aditya Yadav himself and along with Gayatri Batra and Shubham Sharma performed all the experiments and helped in designing several experiments. Chayan K. Nandi guided the complete project and wrote the manuscript with the help of Aditya Yadav, Subrata Ghosh, Deep Jariwala and Eric A. Stach.

Competing interests

The authors declare no competing financial interests.

References

1 X. T. Zheng, A. Ananthanarayanan, K. Q. Luo and P. Chen, *small*, 2015, **11**, 1620–1636.
2 Y. Yan, J. Gong, J. Chen, Z. Zeng, W. Huang, K. Pu, J. Liu and P. Chen, *Adv. Mater.*, 2019, **31**, 1808283.
3 S. Kadian, S. K. Sethi and G. Manik, *Mater. Chem. Front.*, 2021, **5**, 627–658.
4 Q. Liu, J. Sun, K. Gao, N. Chen, X. Sun, D. Ti, C. Bai, R. Cui and L. Qu, *Mater. Chem. Front.*, 2020, **4**, 421–436.
5 H. Li, Z. Kang, Y. Liu and S.-T. Lee, *J. Mater. Chem.*, 2012, **22**, 24230–24253.
6 P. Miao, K. Han, Y. Tang, B. Wang, T. Lin and W. Cheng, *Nanoscale*, 2015, **7**, 1586–1595.
7 S. Zhu, Y. Song, X. Zhao, J. Shao, J. Zhang and B. Yang, *Nano Res.*, 2015, **8**, 355–381.
8 P. Koutsogiannis, E. Thomou, H. Stamatis, D. Gournis and P. Rudolf, *Adv. Phys. X*, 2020, **5**, 1758592.
9 N. C. Verma, A. Yadav and C. K. Nandi, *Nat. Commun.*, 2019, **10**, 2391.
10 R. Zhao, J. Wang, M. Yang, Z. Liu and Z. Liu, *Phys. Chem. Chem. Phys.*, 2013, **15**,

803–806.
11 S. Cheng, J. Yu, T. Ma and N. M. R. Peres, *Phys. Rev. B*, 2015, **91**, 75410.
12 W. Hu, Y. Huang, X. Qin, L. Lin, E. Kan, X. Li, C. Yang and J. Yang, *npj 2D Mater. Appl.*, 2019, **3**, 1–5.
13 D. Pan, J. Zhang, Z. Li and M. Wu, *Adv. Mater.*, 2010, **22**, 734–738.
14 M. Bacon, S. J. Bradley and T. Nann, *Part. & Part. Syst. Charact.*, 2014, **31**, 415–428.
15 X. Zhu, X. Xiao, X. Zuo, Y. Liang and J. Nan, *Part. & Part. Syst. Charact.*, 2014, **31**, 801–809.
16 S. Lai, Y. Jin, L. Shi, R. Zhou, Y. Zhou and D. An, *Nanoscale*, 2020, **12**, 591–601.
17 Z. Gan, H. Xu and Y. Hao, *Nanoscale*, 2016, **8**, 7794–7807.
18 A. Sharma, T. Gadly, A. Gupta, A. Ballal, S. K. Ghosh and M. Kumbhakar, *J. Phys. Chem. Lett.*, 2016, **7**, 3695–3702.
19 L. Pan, S. Sun, A. Zhang, K. Jiang, L. Zhang, C. Dong, Q. Huang, A. Wu and H. Lin, *Adv. Mater.*, 2015, **27**, 7782–7787.
20 B. van Dam, H. Nie, B. Ju, E. Marino, J. M. J. Paulusse, P. Schall, M. Li and K. Dohnalová, *Small*, 2017, **13**, 1702098.
21 J. Hou, W. Wang, T. Zhou, B. Wang, H. Li and L. Ding, *Nanoscale*, 2016, **8**, 11185–11193.
22 X. Wu, F. Tian, W. Wang, J. Chen, M. Wu and J. X. Zhao, *J. Mater. Chem. C*, 2013, **1**, 4676–4684.
23 F. Ehrat, S. Bhattacharyya, J. Schneider, A. Löf, R. Wyrwich, A. L. Rogach, J. K. Stolarczyk, A. S. Urban and J. Feldmann, *Nano Lett.*, 2017, **17**, 7710–7716.
24 M. J. Krysmann, A. Kelarakis, P. Dallas and E. P. Giannelis, *J. Am. Chem. Soc.*, 2011, **134**, 747–750.
25 W.-S. Kuo, X.-C. Shen, C.-Y. Chang, H.-F. Kao, S.-H. Lin, J.-Y. Wang and P.-C. Wu, *ACS Nano*, 2020, **14**, 11502–11509.
26 Y. Zhang, Y. Hu, J. Lin, Y. Fan, Y. Li, Y. Lv and X. Liu, *ACS Appl. Mater. & interfaces*, 2016, **8**, 25454–25460.
27 A. Nandy, A. Kumar, S. Dwivedi, S. K. Pal and D. Panda, *J. Phys. Chem. C*, 2019, **123**, 20502–20511.
28 N. Soni, S. Singh, S. Sharma, G. Batra, K. Kaushik, C. Rao, N. C. Verma, B. Mondal, A. Yadav and C. K. Nandi, *Chem. Sci.*, 2021,**12**, 3615-3626.
29 S. Khan, A. Sharma, S. Ghoshal, S. Jain, M. K. Hazra and C. K. Nandi, *Chem. Sci.*, 2018, **9**, 175–180.
30 V. Strauss, H. Wang, S. Delacroix, M. Ledendecker and P. Wessig, *Chem. Sci.*, 2020, **11**, 8256–8266.
31 W. Kasprzyk, T. Świergosz, S. Bednarz, K. Walas, N. V Bashmakova and D. Bogdał, *Nanoscale*, 2018, **10**, 13889–13894.
32 L. Wang, B. Wu, W. Li, Z. Li, J. Zhan, B. Geng, S. Wang, D. Pan and M. Wu, *J. Mater. Chem. B*, 2017, **5**, 5355–5361.
33 B. Wu, K. Li, F. Sun, J. Niu, R. Zhu, Y. Qian and S. Wang, *Adv. Healthcare Mater.*, 2021,**10**, 2100512.
34 M. Lan, S. Zhao, X. Wei, K. Zhang, Z. Zhang, S. Wu, P. Wang and W. Zhang, *Dye. Pigment.*, 2019, **170**, 107574.
35 M. Lan, L. Guo, S. Zhao, Z. Zhang, Q. Jia, L. Yan, J. Xia, H. Zhang, P. Wang and W. Zhang, *Adv. Ther.*, 2018, **1**, 1800077.
36 J. Zhan, B. Geng, K. Wu, G. Xu, L. Wang, R. Guo, B. Lei, F. Zheng, D. Pan and M. Wu, *Carbon N. Y.*, 2018, **130**, 153–163.
37 W. Li, M. Li, Y. Liu, D. Pan, Z. Li, L. Wang and M. Wu, *ACS Appl. Nano Mater.*, 2018, **1**, 1623–1630.

38 L. Sun, Y. Luo, M. Li, G. Hu, Y. Xu, T. Tang, J. Wen, X. Li and L. Wang, *J. Colloid Interface Sci.*, 2017, **508**, 154–158.

39 S. Bian, C. Shen, H. Hua, L. Zhou, H. Zhu, F. Xi, J. Liu and X. Dong, *Rsc Adv.*, 2016, **6**, 69977–69983.

40 S. Ge, J. He, C. Ma, J. Liu, F. Xi and X. Dong, *Talanta*, 2019, **199**, 581–589.

41 C. Shen, S. Ge, Y. Pang, F. Xi, J. Liu, X. Dong and P. Chen, *J. Mater. Chem. B*, 2017, **5**, 6593–6600.

42 B. Huang, J. He, S. Bian, C. Zhou, Z. Li, F. Xi, J. Liu and X. Dong, *Chinese Chem. Lett.*, 2018, **29**, 1698–1701.

43 J. Qian, C. Shen, J. Yan, F. Xi, X. Dong and J. Liu, *J. Phys. Chem. C*, 2018, **122**, 349–358.

44 Z. Li, F. Bu, J. Wei, W. Yao, L. Wang, Z. Chen, D. Pan and M. Wu, *Nanoscale*, 2018, **10**, 22871–22883.

45 L. Wang, Y. Wang, T. Xu, H. Liao, C. Yao, Y. Liu, Z. Li, Z. Chen, D. Pan, L. Sun and others, *Nat. Commun.*, 2014, **5**, 5357.

46 M. Shamsipur, A. Barati, A. A. Taherpour and M. Jamshidi, *J. Phys. Chem. Lett.*, 2018, **9**, 4189–4198.

47 A. Sharma, T. Gadly, S. Neogy, S. K. Ghosh and M. Kumbhakar, *J. Phys. Chem. Lett.*, 2017, **8**, 5861–5864.

48 P. Zhu, K. Tan, Q. Chen, J. Xiong and L. Gao, *Chem. Mater.*, 2019, **31**, 4732–4742.

49 J. R. Lakowicz, *Principles of fluorescence spectroscopy*, Springer Science & Business Media, 2006.

50 G. S. Kumar, R. Roy, D. Sen, U. K. Ghorai, R. Thapa, N. Mazumder, S. Saha and K. K. Chattopadhyay, *Nanoscale*, 2014, **6**, 3384–3391.

51 R. Ye, Z. Peng, A. Metzger, J. Lin, J. A. Mann, K. Huang, C. Xiang, X. Fan, E. L. G. Samuel, L. B. Alemany and others, *ACS Appl. Mater. & interfaces*, 2015, **7**, 7041–7048.

52 G. Rajender and P. K. Giri, *J. Mater. Chem. C*, 2016, **4**, 10852–10865.

53 J. Du, H. Wang, L. Wang, S. Zhu, Y. Song, B. Yang and H. Sun, *J. Mater. Chem. C*, 2016, **4**, 2235–2242.

54 M. K. Rabchinskii, A. T. Dideikin, D. A. Kirilenko, M. V Baidakova, V. V Shnitov, F. Roth, S. V Konyakhin, N. A. Besedina, S. I. Pavlov, R. A. Kuricyn and others, *Sci. Rep.*, 2018, **8**, 1–11.

55 Y. Kim, Y. Park, S. Han, W. Park, M. Kim, K. Kim, J. Joo, S. K. Hahn and W. Kwon, *Nanomaterials*, 2022, **12**, 70.

56 E. V Kundelev, N. V Tepliakov, M. Y. Leonov, V. G. Maslov, A. V Baranov, A. V Fedorov, I. D. Rukhlenko and A. L. Rogach, *J. Phys. Chem. Lett.*, 2020, **11**, 8121–8127.

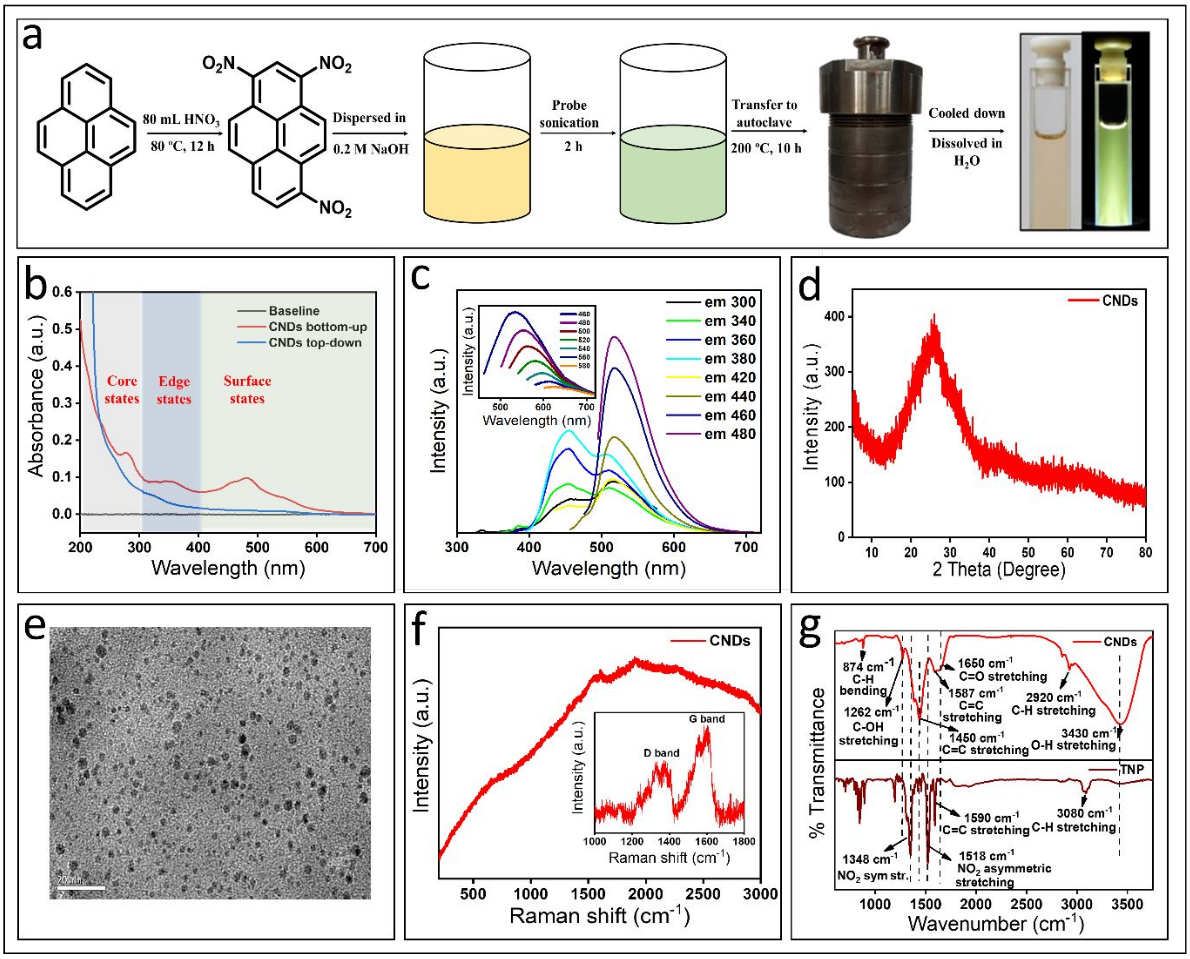

Fig. 1 (a) Schematics of the synthesis of CNDs derived from pyrene. (b) A comparison of the absorption spectra (red color) of CNDs synthesized from pyrene via bottom-up approach and (blue color) from graphite via top-down approach. (c) Excitation independent emission spectra of CNDs derived from pyrene via bottom-up approach, (inset) excitation dependent emission in CNDs synthesis from graphite via top-down approach. (d) PXRD spectrum with a broad peak at ~26 degrees. (e) Representative TEM image of CNDs (scale bar 20 nm). (f) Raman spectrum shows the maximum fluorescence background, (inset) shows the signature of typical D and G bands after baseline correction. (g) Comparison of the FTIR spectra of CNDs and TNP.

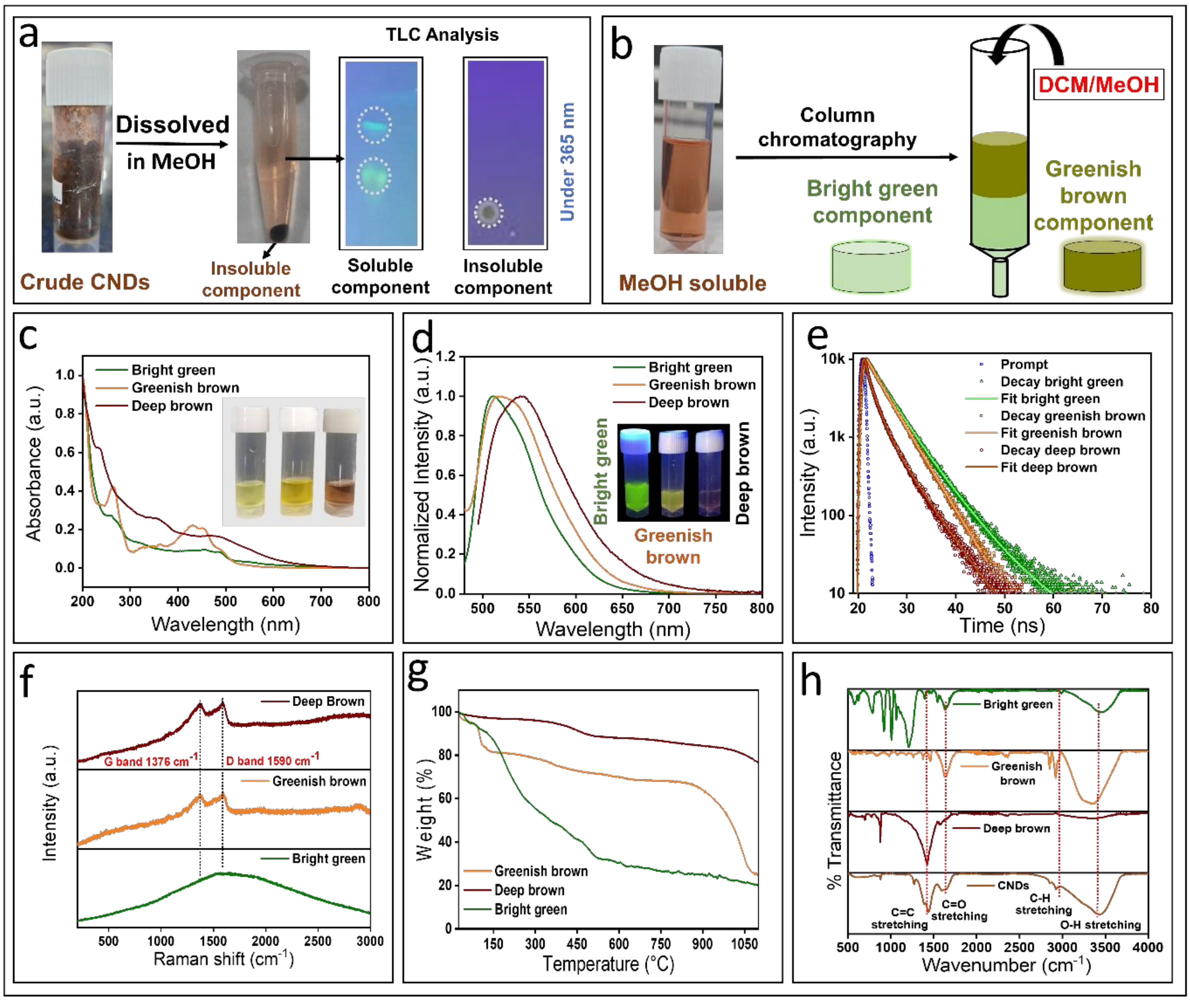

Fig. 2 (a) Detail schematic of the MeOH solvent extracted separation of crude CNDs. (b) Schematic of column chromatographic separation of MeOH soluble components. (c) A comparison of the absorption spectra of all three separated components, (inset) naked eye image of the components. (d) Normalized steady-state fluorescence emission spectra of all separated components, (inset) show the 365 UV light illuminated color. (e) Lifetime decay of all three components with bright green component showing maximum lifetime and deep brown component showing the lowest lifetime. (f) Raman spectra of the separated components: bright green component shows only the fluorescence background without D and G bands while greenish brown and deep brown components show prominent D and G bands. (g) TGA spectra suggesting completely different thermal stability of each of the components. (h) Comparison of the FTIR spectra of crude CNDs and all separated components.

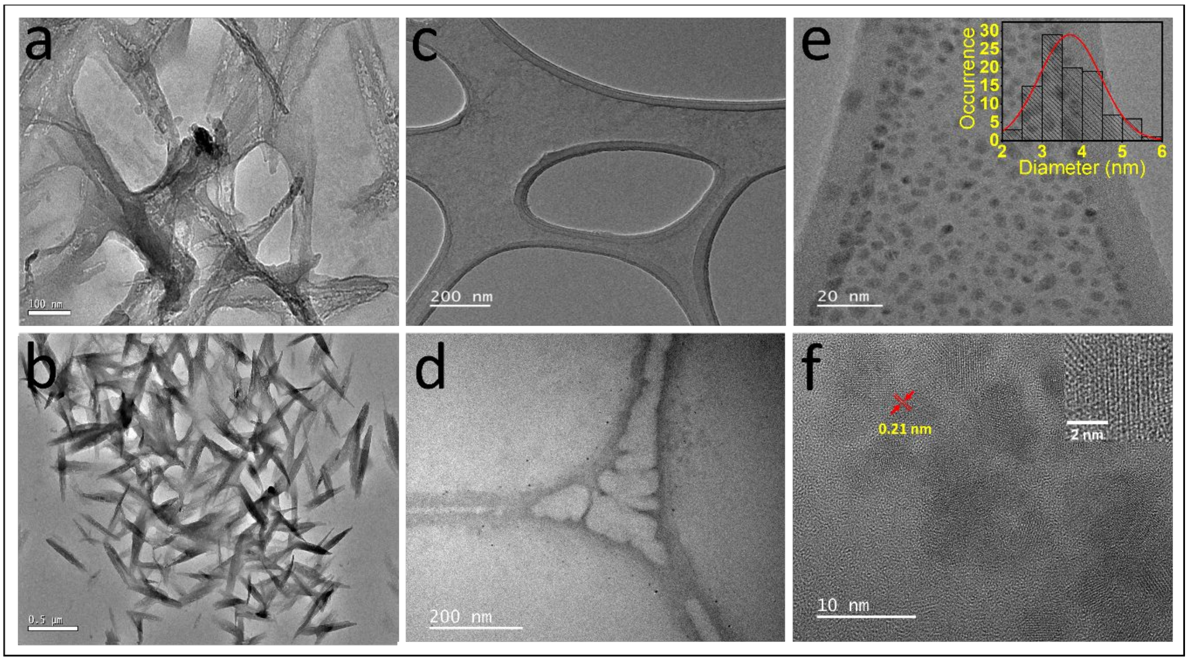

Fig. 3 TEM images of (a-b) bright green, (c-d) greenish brown and (e-f) deep brown component. Bright green component shows different types of aggregated structure under different experimental conditions but without any CNDs formation. Different morphologies appeared due to concentration dependent drying mediated process during sample preparation. The greenish brown component also shows no significant evidence of dot formation under TEM imaging while deep brown component shows proper dot-like structures.

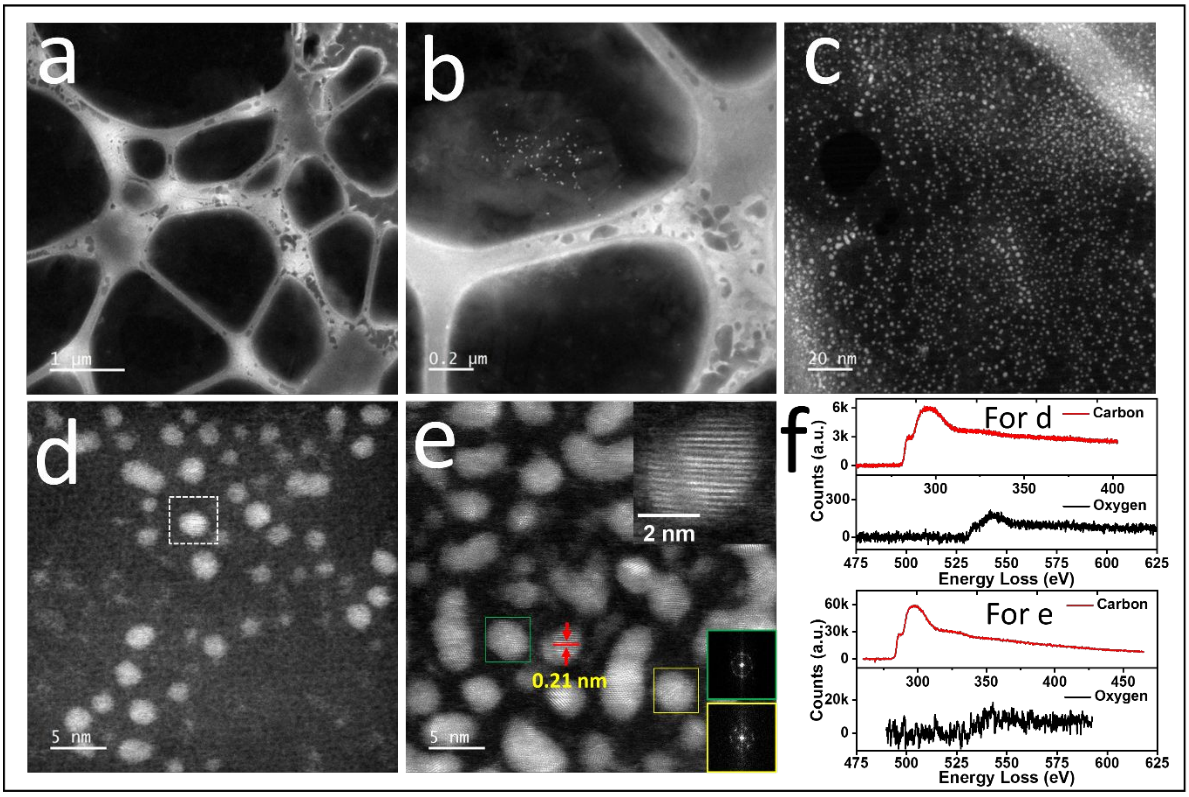

Fig. 4 (a-c) Low magnification STEM images of the bright green (a), greenish brown (b) and deep brown component (c). (d-e) are the high magnification and high-resolution images of greenish brown (d) and deep brown components (e). Lattice fringes in the STEM contrast can be clearly seen on the particles in (e) with an inset showing Fourier transform pattern suggesting some crystalline order. (f) Electron energy loss spectra (EELS) from d (top) and e (bottom) respectively. A strong oxygen signature is observed in EELS spectra from greenish brown sample (d) suggesting a hybrid structure of carbogenic core covered with oxygen containing organic functional groups on the surface.

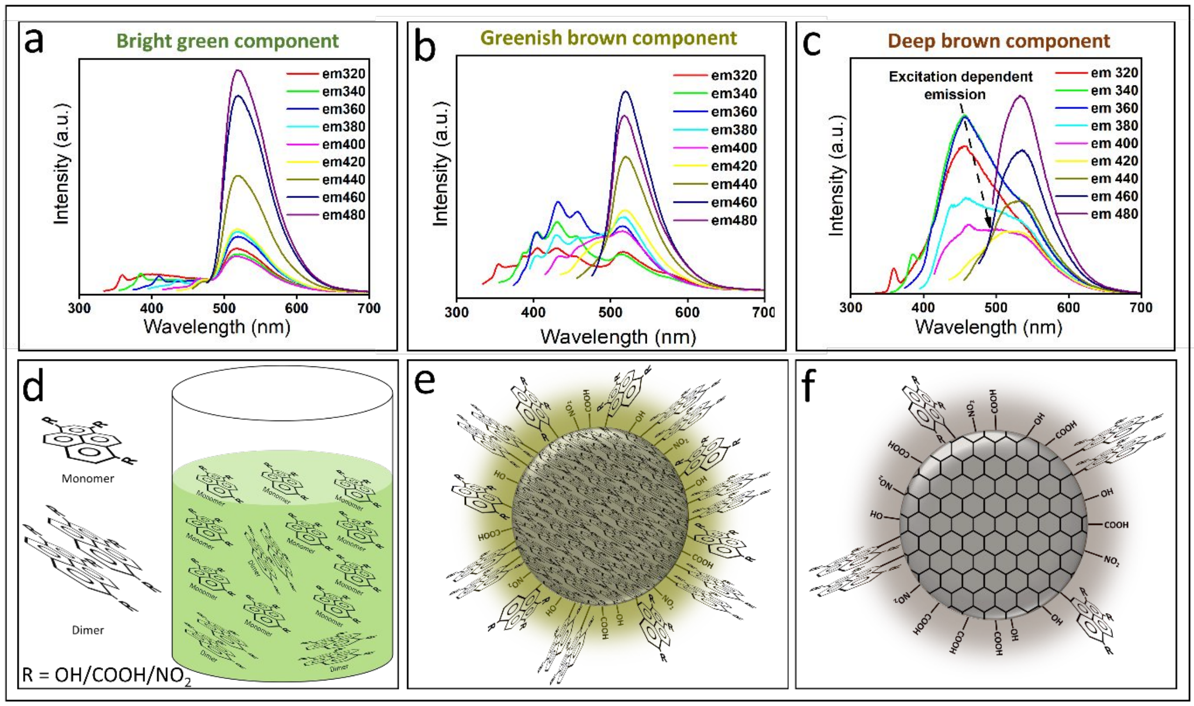

Fig. 5 Excitation wavelength dependent emission spectra: (a) Bright green component shows excitation independent emission only above 500 nm with a peak maximum at 515 nm. (b) Greenish brown component shows two emission features with excitation independent emission above 500 nm with a maximum at 525 nm and structured but excitation independent emission below 500 nm. (c) Deep brown component shows almost equally intense excitation wavelength independent emission with maximum at 541 nm and excitation dependent emission with a peak maximum at around 450 nm. (d-f) Proposed structure of bright green, greenish brown and deep brown components.

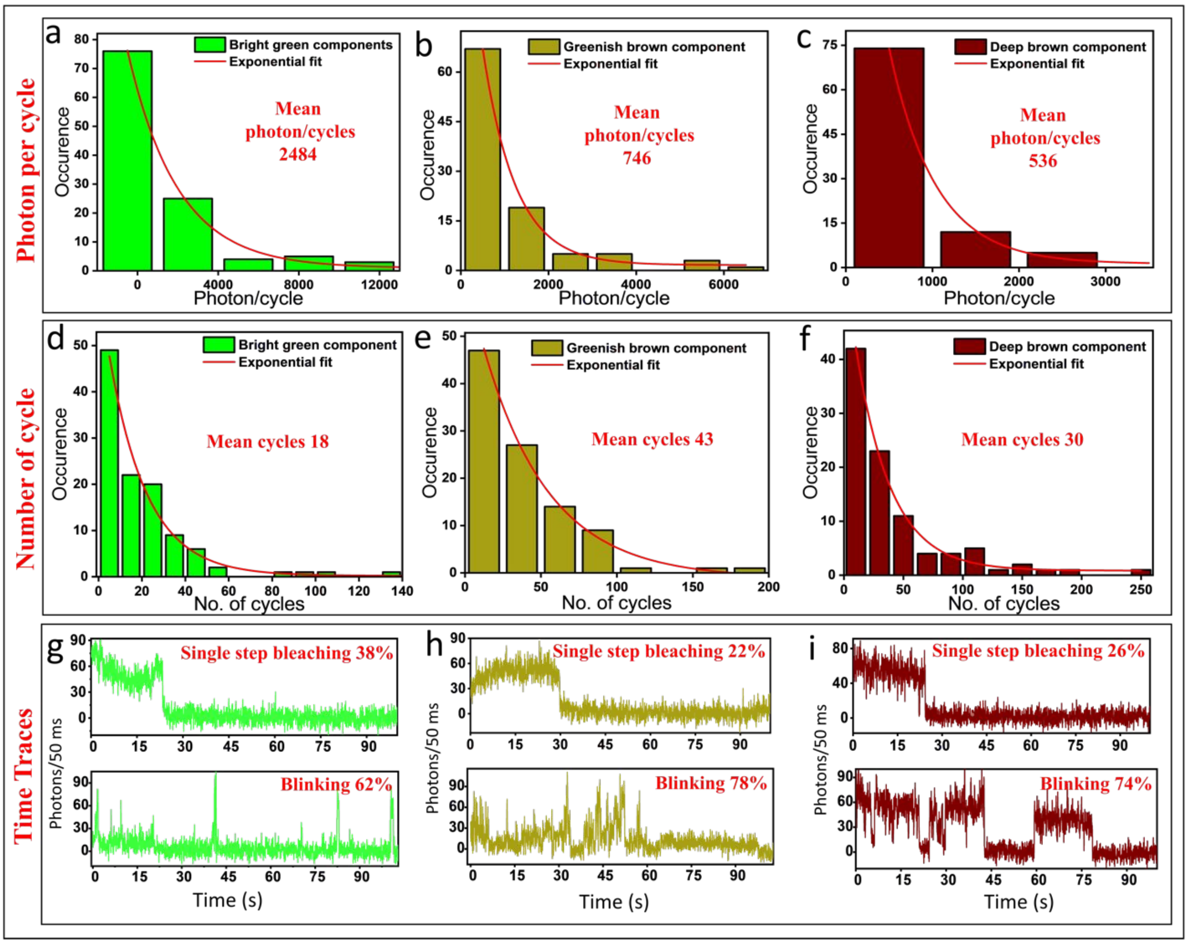

Fig. 6 Measured single-particle level (a-c) photons counts/cycle, (d-f) number of ON-OFF switching cycles for each of the separated components. The maximum photon counts/cycle was observed for the bright green component, while least photon counts/cycle was observed for deep brown component. (g-i) Single-particle time traces of both single-step bleaching and blinking events.